Proceedings of the ASME 2014 International Design Engineering Technical Conferences & Computers and Information in Engineering Conference
IDETC/CIE 2014
August 17-20, 2014, Buffalo, New York, USA

DETC2014-35155

DIMENSIONAL SYNTHESIS OF A NOVEL 2T2R PARALLEL MANIPULATOR FOR MEDICAL APPLICATIONS

Nitish Kumar*
ICube laboratory - UMR 7357
University of Strasbourg
Strasbourg, France
and
IHU Strasbourg
Strasbourg, France
Email: nitish.kumar@etu.unistra.fr

Olivier Piccin
ICube laboratory - UMR 7357
University of Strasbourg
Strasbourg, France
and
INSA Strasbourg
Strasbourg, France
Email: olivier.piccin@insa-strasbourg.fr

Bernard Bayle
ICube laboratory - UMR 7357
University of Strasbourg
Strasbourg, France
and
IHU Strasbourg
Strasbourg, France
Email: bernard.bayle@unistra.fr

ABSTRACT

This paper deals with the dimensional synthesis of a novel parallel manipulator for medical applications. This parallel mechanism has a novel 2T2R mobility derived from the targeted application of needle manipulation. The kinematic design of this 2T2R manipulator and its novelty are illustrated in relation to the percutaneous procedures. Due to the demanding constraints on its size and compactness, achieving a large workspace especially in orientation, is a rather difficult task. The workspace size and kinematic constraint analysis are considered for the dimensional synthesis of this 2T2R parallel mechanism. A dimensional synthesis algorithm based on the screw theory and the geometric analysis of the singularities is described. This algorithm also helps to eliminate the existence of voids inside the workspace. The selection of the actuated joints is validated. Finally, the dimensions of the structural parameters of the mechanism are calculated for achieving the required workspace within the design constraints of size, compactness and a preliminary prototype without actuators is presented.

1 INTRODUCTION

Interventional radiology is a medical specialty where the use of surgical needles is very common. One of the key movements of the radiologist is the needle manipulation in free space, which encompasses the wide range of procedures that require needle insertion such as biopsies, radiofrequency ablations. Among the various imaging modalities available, computed tomography (CT) provides a rather fast and accurate visual feedback to the radiologist. However, repeated exposure to X-rays endangers radiologist's health. This is the principal motivation for developing teleoperated robotic assistants to remotely insert needles under CT guidance. In most existing systems, needle manipulation and insertion task are kept separate [1, 2, 3], with a needle insertion driver mounted on the platform of a needle manipulation device.

These robotic systems are placed in the tunnel of the CT scanner for the image-guided needle manipulation. After introduction of the patient in the tunnel, there is very scarce space left for placing a robotic device. This requires such robotic devices to be very small in size and compact in form. In addition to such constraints, a large workspace, especially in orientation, is required for the manipulation of the needle, which is a difficult design challenge. Most of these robotic devices which are mounted on the patient have a parallel architecture.

Parallel mechanisms (PMs) have several advantages which include higher stiffness, higher precision and compactness. But they suffer from the disadvantages of smaller workspace and the presence of singularities, both serial and parallel. The workspace and the singularities are both very sensitive to the structural pa-

*Address all correspondence to this author.

Copyright © 2014 by ASME

Downloaded From: http://proceedings.asmedigitalcollection.asme.org/ on 06/15/2018 Terms of Use: http://www.asme.org/about-asme/terms-of-use

rameters of the PM. Hence, a proper dimensional synthesis of the PMs, which involves finding dimensions of its structural parameters subject to design constraints and objectives, is very important. Most of these algorithms for dimensional synthesis are based on the evaluation of performance indices like isotropy index, transmission index, manipulability [4] or condition number [5].The major drawback with these algorithms is that their complexity increases rapidly with the number of structural parameters, as the effect of each structural parameter has to be analyzed by numerical computation of the Jacobian while discretizing the parameter space. Algorithms based on the kinematic mapping [6] and kinematic constraints [7] of the mechanism provide another alternative. In the works [8, 9], visual approach using specific trajectory and motion planning as criteria has proven successful for design of planar mechanisms where motion description is simpler. This approach relies on the kinematic mapping from Cartesian to planar quaternions to express the kinematic constraints as constraint manifolds. It is not yet adapted for spatial parallel mechanisms like the 2T2R mechanism discussed in this paper. The 2T2R parallel mechanism has complex spatial motion owing to its higher degree of freedom (DOF). It has constraints on the workspace size as opposed to any trajectory specific constraints due to nature of the targeted application. Moreover, the trajectory specification through specific points for the planar mechanism is equivalent to set of points representing the workspace and its size for a spatial mechanism. Therefore in this paper, kinematic constraint analysis and the workspace size are considered for the dimensional synthesis algorithm presented in this paper. The kinematic constraints of a serial, closed loop or parallel mechanism, which constrain its motion, can be described by its singularities. Using screw theory, it is possible to enumerate and describe these kinematic constraints geometrically in the vectorial form. This form is independent of the choice of kinematic mapping and parametrization used for representing intermediate reference frames of the mechanism. This leaves an open choice for use of either quaternions, Euler angles, Cartesian co-ordinates or a user-defined one, for kinematic mapping in order to represent the end-effector reference frame. Also, for parametrization of the intermediate reference frames, one has open choice of using either Denavit-Hartenberg (DH) or using twists with screw motion.

This paper is organized into seven sections. In section 2, a novel mechanism featuring a novel 2T2R mobility is presented for the needle manipulation task. In section 3, the algorithm for the dimensional synthesis of the 2T2R PM, based on geometric analysis of its singularities with the help of screw theory, is described. In section 4, the design constraints and the modeling of the 2T2R PM is presented. In section 5, with the help of the modeling based on DH parameters, singularity plots are generated for each leg of the PM and dimensions of the structural parameters are calculated for achieving the desired workspace size. In section 6, the important structural parameters of the 2T2R PM are summarized and a fabricated prototype is presented. Finally, conclusion and perspectives of the current research work are laid out in section 7.

2 A NOVEL 2T2R MECHANISM FOR NEEDLE MANIPULATION

This section introduces a novel 2T2R manipulator [10] synthesized with the help of screw theory and featuring a wrench system derived from the task of needle manipulation. The needle manipulation task requires a robotic device with a minimum of 4-DOF mobility, two for the translation of the needle axis and two for its orientation. Therefore, lower mobility PMs are natural candidates for fulfilling the needle manipulation requirements. In the literature, several parallel robotic systems have been proposed for needle manipulation but often they have fewer [2] or more [11] than the minimum required DOFs. Very few such systems with the 4-DOF [3] have been developed and among these robotic systems, none of them features a center of rotation which ideally should coincide with the entry point on surface of the skin. The presence of such a remote center of motion allows the orientation of the device without causing any surface tissue lacerations, when the needle is slightly inserted into the body.

The Fig. 1, shows a simplified CAD model of the 2T2R PM. It consists of three legs, each having five revolute joints. Overall, there are two leg types corresponding to two different wrench systems. Twists and wrenches of pitch h are denoted as $\$^h$ and $\hat{\$}^h$ respectively. Accordingly, the wrench systems of order n formed by zero and infinite pitch wrenches are denoted as n-$\hat{\$}^0$ and n-$\hat{\$}^\infty$. The first type leg (Leg 1) provides a constraint with a 1-$\hat{\$}^0$

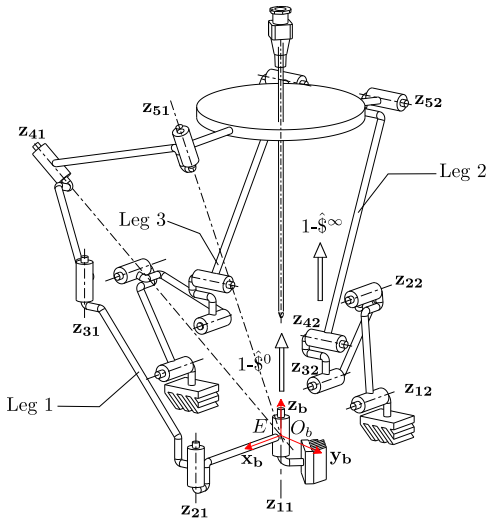

FIGURE 1: 2T2R MANIPULATOR IN ITS REFERENCE CONFIGURATION.

Copyright © 2014 by ASME

Downloaded From: http://proceedings.asmedigitalcollection.asme.org/ on 06/15/2018 Terms of Use: http://www.asme.org/about-asme/terms-of-use

wrench system and the second type legs (Leg 2 and Leg 3) provide two constraints with a 1-$\hat{\$}^{\infty}$ wrench system. With this arrangement, the leg 1 restricts one translational DOF, whereas the legs 2 and 3 restrict one rotational DOF. The wrench system of the 2T2R PM is obtained as 1-$\hat{\$}^{0}$-1-$\hat{\$}^{\infty}$. A more comprehensive description of the constraint wrenches for the mechanism is provided in the next section. Few PMs with 2T2R mobility have been reported in the literature. For example, the mechanisms presented in [12, 13] have wrench systems that does not match the one requested by the needle manipulation task discussed in this paper. The overconstraint for this 2T2R PM is due to the presence of the extra leg 3 which provides a redundant first order wrench system 1-$\hat{\$}^{\infty}$. Thus the number of overconstraints ν is equal to one. Let the set of joints having parallel axes be denoted by $()_p$ and the set of joints having axes intersecting in one point be denoted by $()_i$. With this notation the PM would be referred to as a 1-$(RRR)_p(RR)_i$–2-$(RRR)_p(RR)_p$ architecture. As indicated in the Fig. 1, the set of axes $(RR)_i$ in leg 1 intersects at the entry point E, which also serves as the center of rotation for the PM.

Each of the three legs has five revolute joints. Considering a joint i in the leg k ($i = 1\ldots5, k = 1\ldots3$), let $\mathbf{z_{ik}}$ as shown in Fig. 1 and $\mathbf{t_{ik}}$, represent the direction of the joint axis and the position vector directed from O_b to any point on the joint axis, respectively. With this representation, the twist of the i^{th} joint of leg k is $\$^0_{ik} = \left[\mathbf{z_{ik}}\ \mathbf{t_{ik}} \times \mathbf{z_{ik}}\right]^T$. If the axes of $\$^0_{ik}$ and $\$^0_{jk}$ form a plane, it would be referred to as Π_{ijk}.

As four inputs are needed to control this 2T2R PM with three legs, one of the legs needs to be assigned two inputs. One input is assigned to each $(RRR)_p(RR)_p$ leg and is located at the first revolute joint, namely $\mathbf{z_{12}}$, $\mathbf{z_{13}}$ connected to the base, whereas the other two inputs are assigned to the $(RRR)_p(RR)_i$ leg and are located at the first two joints starting from the base, namely $\mathbf{z_{11}}$, $\mathbf{z_{21}}$, as shown in Fig. 1. The first representative axis $\mathbf{z_{11}}$ will be realized by a circular prismatic joint in the actual prototype. Hence, the second actuator, though floating over the circular joint, would be practically on the base.

The mobility of this PM composed of n bodies connected by g joints, each with f_i DOFs, using the modified Kutzbach–Grübler criterion [14], is verified to be 4:

$$m = 6(n-g-1)+\sum_{i=1}^{g} f_i + \nu = 6(14-15-1)+15+1 = 4. \quad (1)$$

As expected, this 2T2R mechanism allows the translation of the entry point E in a planar zone of operation $(O_b, \mathbf{x_b}, \mathbf{y_b})$. After fixing the entry point to the desired position, the mechanism allows rotation in two directions to achieve the targeted orientation of the needle axis around the entry point which serves as the center of rotation for the device.

3 DIMENSIONAL SYNTHESIS METHODOLOGY

The dimensional synthesis of this PM is based on the objective criterion of achieving the required workspace size, while maintaining the system compactness within certain limits. The needle manipulation in free space can be regarded as the alignment of the needle's axis with the axis of insertion such that it passes through the entry point on the patient's skin. This whole task can be decomposed in two sequential steps, first the translation of the needle axis to match the entry point and the subsequent orientation of the needle axis about this entry point. Hence, the workspace definition for needle manipulation can be considered to be the union of the constant-orientation translation workspace and of the constant-position orientation workspace. One interesting aspect is that such workspace of a PM is the intersection of the workspace of its individual legs, which can be studied independently [15]. This special property removes any coupling between the structural parameters of the different legs and thus it simplifies the dimensional synthesis of the PM.

As the legs of the PM have only revolute joints, the workspace boundary of each leg is the locus of its singularities [16]. Thus the workspace of the 2T2R mechanism can be generated by plotting the loci of its singularity curves. The workspace size is limited by its external and internal boundaries. Where external boundaries need to be modified, the internal boundaries namely the voids need to be eliminated. Also, the additional curves due to the presence of parallel singularities need to be investigated. Thus, the velocity equation for the 2T2R PM ($\mathbf{J_X}\dot{\mathbf{X}} = \mathbf{J_q}\dot{\mathbf{q}}$) needs to be considered for discussion of its singularities. The full direct Jacobian $\mathbf{J_X}$ can be obtained by stacking the four actuation wrenches $\hat{\$}_{i,a}$ and the two constraint wrenches $\hat{\$}_{j,c}$ of the 2T2R PM. The four actuation wrenches can be expressed as $\hat{\$}_{i,a} \equiv \left[\mathbf{s_i}\ \mathbf{r_i} \times \mathbf{s_i}\right]^T$ where $\mathbf{s_i}$ denotes the direction of the actuation wrench and $\mathbf{r_i}$ is the position vector directed from origin the O_b to a point of the wrench axis. The two constraint wrenches $\hat{\$}_{j,c}$ produced by the mechanism have the form $\hat{\$}_{1,c} \equiv \left[\mathbf{z_b}\ \mathbf{O_bE} \times \mathbf{z_b}\right]^T$ and $\hat{\$}_{2,c} \equiv \left[\mathbf{0}\ \mathbf{m_1}\right]^T$ where $\mathbf{m_1}$ is the direction of the wrench system 1-$\hat{\$}^{\infty}$. Therefore, the $\mathbf{J_X}$ and $\mathbf{J_q}$ matrices of the 2T2R PM can be displayed as :

$$\mathbf{J_X} = \begin{bmatrix} \mathbf{s_1} & \mathbf{r_1}\times\mathbf{s_1} \\ \mathbf{s_2} & \mathbf{r_2}\times\mathbf{s_2} \\ \mathbf{s_3} & \mathbf{r_3}\times\mathbf{s_3} \\ \mathbf{s_4} & \mathbf{r_4}\times\mathbf{s_4} \\ \mathbf{z_b} & \mathbf{O_bE}\times\mathbf{z_b} \\ \mathbf{0} & \mathbf{m_1} \end{bmatrix} \quad \mathbf{J_q} = \begin{bmatrix} \hat{\$}_{1,a}\cdot\$^0_{11} & 0 & 0 & 0 & 0 \\ 0 & \hat{\$}_{2,a}\cdot\$^0_{21} & 0 & 0 & 0 \\ 0 & 0 & \hat{\$}_{3,a}\cdot\$^0_{12} & 0 & 0 \\ 0 & 0 & 0 & \hat{\$}_{4,a}\cdot\$^0_{13} & 0 \\ 0 & 0 & 0 & 0 & 0 \\ 0 & 0 & 0 & 0 & 0 \end{bmatrix}$$

The parallel and serial singularities occur when rank of $\mathbf{J_X}$ and $\mathbf{J_q}$ is less than six and four respectively but neither the symbolic form of $\mathbf{J_X}$, nor of $\mathbf{J_q}$ allow to derive the simplest representation of singularity conditions.

In the further subsections, a screw theory based inspection is used to obtain the geometrical form of the singularities, as this

Copyright © 2014 by ASME

Downloaded From: http://proceedings.asmedigitalcollection.asme.org/ on 06/15/2018 Terms of Use: http://www.asme.org/about-asme/terms-of-use

form is independent of the choice of the parametric representation and produces the simplest expression with the minimal number of structural parameters.

3.1 Serial Singularity Analysis of Individual Legs

As the legs 2 and 3 are kinematically identical, only serial singularities of legs 1 and 2 are discussed. The leg 1 is made up of two sub-units, $(RRR)_p$ and $(RR)_i$. The twist system of leg 1 is the union of the twist system of these two sub-units. The twist system of the $(RRR)_p$ and $(RR)_i$ units is 1-$\$^0$-2-$\$^\infty$ and 2-$\$^0$ respectively. Hence, the twist system of this leg is 3-$\$^0$-2-$\$^\infty$. Applying the principle of reciprocity, its wrench system is derived as 1-$\hat{\$}^\infty$. Aside from this constraint wrench, extra constraint wrenches develop when the leg 1 is in singularity. The following conditions characterize the singularity of leg 1 :

Singularity-11 (Fig. 2(a)): When the normal to the plane Π_{451} is perpendicular to $\mathbf{z_{31}}$:

$$(\mathbf{z_{41}} \times \mathbf{z_{51}}) \cdot \mathbf{z_{31}} = 0 \tag{2}$$

In this case, the twist system of the leg degenerates to 2-$\$^0$-2-$\$^\infty$. The extra constraint moment, denoted as $\hat{\$}^\infty_{11,c}$, at singularity is shown in Fig. 2(a).

Singularity-21 (Fig. 2(b)) : When three joint axes $\mathbf{z_{11}}$, $\mathbf{z_{21}}$ and $\mathbf{z_{31}}$ are coplanar:

$$(\mathbf{t_{31}} - \mathbf{t_{21}}) \times (\mathbf{t_{21}} - \mathbf{t_{11}}) = 0 \tag{3}$$

This is the well-known elbow singularity occurring in serial mechanisms with revolute joints. In this case, the twist system of the leg degenerates to 3-$\$^0$-1-$\$^\infty$. The extra constraint force $\hat{\$}^0_{21,c}$ at singularity is shown in Fig. 2(b).

The leg 2 is made up of two sub-units, $(RRR)_p$ and $(RR)_p$. The twist system of the $(RRR)_p$ and $(RR)_p$ units is 1-$\$^0$-2-$\$^\infty$ and 1-$\$^0$-1-$\$^\infty$ respectively. The wrench system of the leg 2 is derived as 1-$\hat{\$}^\infty$. The following conditions characterize the singularity of leg 2 :

Singularity-12 (Fig. 2(c)): When the normal to the plane Π_{452} is perpendicular to $\mathbf{z_{32}}$:

$$[(\mathbf{t_{52}} - \mathbf{t_{42}}) \times \mathbf{z_{42}}] \cdot \mathbf{z_{32}} = 0 \tag{4}$$

In this case, the twist system of the leg degenerates to 2-$\$^0$-2-$\$^\infty$. The extra constraint force $\hat{\$}^0_{12,c}$ at singularity is shown in Fig. 2(c).

Singularity-22 (Fig. 2(d)): This elbow singularity occurs, when $\mathbf{z_{12}}$, $\mathbf{z_{22}}$ and $\mathbf{z_{32}}$ are coplanar:

$$(\mathbf{t_{32}} - \mathbf{t_{22}}) \times (\mathbf{t_{22}} - \mathbf{t_{12}}) = 0 \tag{5}$$

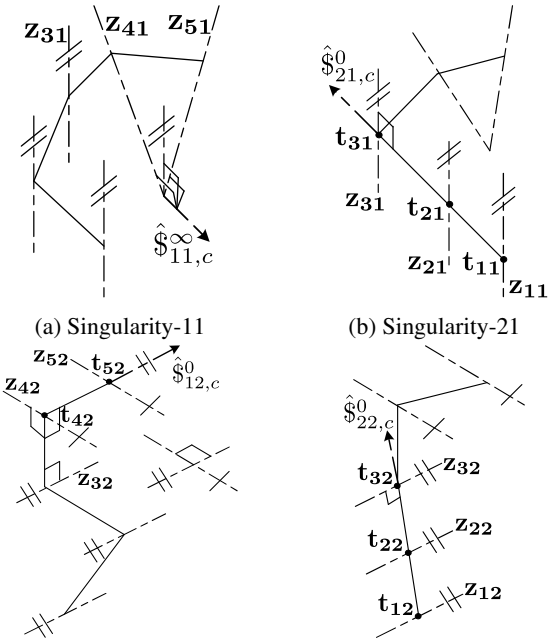

(a) Singularity-11 (b) Singularity-21

(c) Singularity-12 (d) Singularity-22

FIGURE 2: SINGULARITIES FOR LEGS 1 AND 2.

In this case, the twist system of the leg degenerates to 2-$\$^0$-2-$\$^\infty$. The extra constraint force $\hat{\$}^0_{22,c}$ at singularity is shown in Fig. 2(d).

3.2 Parallel Singularity Analysis And Selection of Actuated Joints

With the notations defined in section 2, a geometric interpretation of the actuation wrench system 4-$\hat{\$}_a$ can be obtained. The actuation wrenches $\hat{\$}_{1,a}$ and $\hat{\$}_{2,a}$ are each defined by the intersection of the planes taken in the pairs (Π_{231}, Π_{451}) and (Π_{131}, Π_{451}). Thus, it can be concluded that $\hat{\$}_{1,a}$ and $\hat{\$}_{2,a}$ both lie on the plane Π_{451} and hence must intersect each other if not parallel to each other. Thus $\hat{\$}_{1,a}$–$\hat{\$}_{2,a}$ forms a planar pencil of lines. Similarly, actuation wrenches $\hat{\$}_{3,a}$ and $\hat{\$}_{4,a}$ are defined respectively by the intersection of the planes in the pairs (Π_{232}, Π_{452}) and (Π_{233}, Π_{453}). The constraint wrench $\hat{\$}_{1,c}$ is a line passing through O_b and parallel to $\mathbf{z_b}$. The constraint wrench $\hat{\$}_{2,c}$ is a line orthogonal to the axes quintuple $(\mathbf{z_{12}}, \mathbf{z_{22}}, \mathbf{z_{32}}, \mathbf{z_{42}}, \mathbf{z_{52}})$. The conditions for the parallel singularity of 2T2R PM are:

1. The wrenches $\hat{\$}_{1,a}$ and $\hat{\$}_{2,a}$ become coincident. This condition occurs whenever the planes (Π_{231},Π_{131}) become coincident. This condition is identical to the serial elbow singularity of leg 1 expressed in Eqn. (3).

Copyright © 2014 by ASME

Downloaded From: http://proceedings.asmedigitalcollection.asme.org/ on 06/15/2018 Terms of Use: http://www.asme.org/about-asme/terms-of-use

2. The wrenches $\hat{\$}_{3,a}$ and $\hat{\$}_{4,a}$ become coincident.

$$\hat{\$}_{3,a} = \pm\hat{\$}_{4,a} \tag{6}$$

This condition occurs whenever the planes in both pairs (Π_{232},Π_{233}) and (Π_{452},Π_{453}) become coincident. Certain platform configurations can always be found where the planes in pair (Π_{232},Π_{233}) are coincident. But if the planes in the pair (Π_{452},Π_{453}) are put non coincident in the reference assembly configuration, they remain non coincident for every platform configuration. Hence, this parallel singularity can be avoided by choosing different structural parameters defining the point of placement of legs 2 and 3 on the base, as expressed later in Eqn. (9). Greater the difference in these structural parameters, better will be the distance from this parallel singularity.

3. There is no constraint singularity as $\hat{\$}_{1,c}$ and $\hat{\$}_{2,c}$ are linearly independent in every configuration.

As these parallel singularities can be avoided for the 2T2R PM, only serial singularities will be discussed for its dimensional synthesis. Since, the matrix $\mathbf{J_X}$ is singular only for some specific configurations of the platform and not for every configuration, the choice of the actuated joints is valid.

3.3 Algorithm

The algorithm used for the dimensional synthesis of this 2T2R PM can be described as follows :

Step 1: Derivation of the singularity conditions both serial and parallel from a screw based inspection as opposed to derivation from the symbolic form of the matrix $\mathbf{J_X}$ or $\mathbf{J_q}$, as it will lead to the simplest form for the singularity conditions.
Step 2: Use of DH parameters and resolution of the inverse kinematics to obtain the equations relating the operational coordinates and the structural parameters, corresponding to each singularity.
Step 3: Division of the singularity equations to separate curves corresponding to voids and curves corresponding to external boundaries.
Step 4: Modification of the singularity curves.

(a) Eliminate or minimize the void formation
(b) Optimize or extend the external boundaries up to the required limits

Step 5: Resolution of above equations corresponding to the singularity curves in order to find the set of DH parameters for the mechanism while satisfying the design constraints and objectives.

Even with these Eqn. (2)-(5), the problem of the dimensional synthesis is underconstrained and one needs to put some design constraints which in our case would correspond to overall size of the 2T2R PM and the avoidance of the parallel singularity condition Eqn. (6). The complexity of this algorithm does not increase much with increase in the number of structural parameters. Also, this algorithm can identify and localize sensitive structural parameters to each singularity curve. It will be evident in later sections, that each of Eqn. (2)- (5) could be reduced to cosine or sine of angles θ obtained from solution of the inverse kinematics. Hence, for this algorithm to work, a closed-form solution of the inverse kinematics is necessary to obtain the analytical expressions for the singularities. However, the full derivation of the inverse kinematics for the 2T2R PM is not developed in this paper, rather the developed expressions for the singularities and their plots will be given in next sections.

4 MODELING AND DESIGN CONSTRAINTS

4.1 Mathematical Modeling

As the legs 2 and 3 are identical, the models for only legs 1 and 2 are described. For the mathematical modeling of this 2T2R PM, the modified Denavit-Hartenberg parameters [17] are used, since it can readily take into account mechanisms with closed chains or parallel architecture. As a typical example, some of the important DH parameters are shown in the Fig. 3 for the legs 1 and 2, whereas the complete list of DH parameters is given in the Tab. 1. The reference frames $\mathscr{R}_{pk}$ are intermediate frames other than the base frame, which help to position the point of attachment of each leg on the base. $\mathscr{R}_{fk}$ are the frames attached to the end-effector of the 2T2R manipulator, which help to derive the loop-closure relations. The angle θ_{rik} is the i^{th} angle between the successive x-axes of the DH model, in the reference configuration of the leg k. The notation for the parameters of the leg-3 would follow those of leg-2, with the subscript $k = 3$.

From the Tab. 1, the set of design parameters $\mathscr{D}_{P_1}$ for leg 1 is given in Eqn. (7a). Some design constraints $\mathscr{D}_{C_1}$, given in

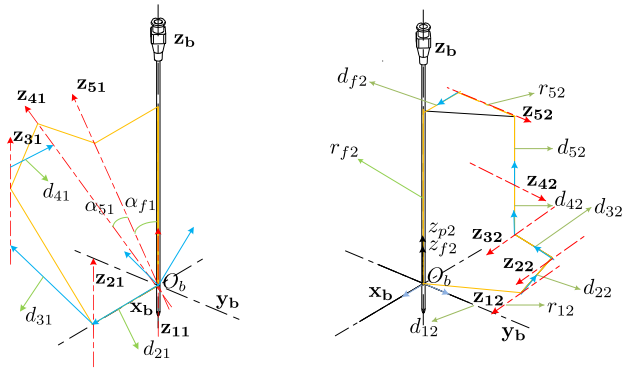

(a) for leg 1 (b) for leg 2

FIGURE 3: MODIFIED DH PARAMETERS.

Copyright © 2014 by ASME

Downloaded From: http://proceedings.asmedigitalcollection.asme.org/ on 06/15/2018 Terms of Use: http://www.asme.org/about-asme/terms-of-use

TABLE 1: DH PARAMETERS.

(a) for leg 1

θ_{i1}	α_{i1}	d_{i1}	r_{i1}
$\theta_{p1}=0$	0	0	0
$\theta_{r11}=0$	0	0	0
$\theta_{r21}=-\frac{\pi}{2}$	0	d_{21}	0
θ_{r31}	0	d_{31}	r_{31}
θ_{r41}	α_{41}	d_{41}	r_{41}
θ_{r51}	α_{51}	0	0
$\theta_{f1}=\frac{\pi}{2}$	α_{f1}	0	0

(b) for leg 2

θ_{i2}	α_{i2}	d_{i2}	r_{i2}
$\theta_{p2}=\frac{\pi}{2}$	0	0	r_{p2}
θ_{r12}	$\pi/2$	d_{12}	r_{12}
θ_{r22}	0	d_{22}	0
θ_{r32}	0	d_{32}	0
θ_{r42}	$\pi/2$	d_{42}	0
θ_{r52}	0	d_{52}	r_{52}
$\theta_{f2}=0$	$\pi/2$	d_{f2}	r_{f2}

Eqn. (7b), are also imposed to take into account the size of the PM and to avoid obtaining values practically difficult to realize.

$$\mathscr{D}_{P_1} = \{\theta_{r31}, \theta_{r41}, \theta_{r51}, \alpha_{41}, \alpha_{51}, \alpha_{f1}, d_{21}, d_{31}, d_{41}, r_{31}, r_{41}\} \quad (7a)$$

$$\mathscr{D}_{C_1} = \{d_{21} \leq 50 \text{ mm}, \quad \alpha_{i1} \leq \frac{\pi}{4}\} \quad (7b)$$

The design parameters $\mathscr{D}_{P_2}$ and the design constraints $\mathscr{D}_{C_2}$ for leg 2 are given in Eqn. (8a) and Eqn. (8b), respectively.

$$\mathscr{D}_{P_2} = \{\theta_{r12}, \theta_{r22}, \theta_{r32}, \theta_{r42}, \theta_{r52}, d_{12}, d_{22}, d_{32}, d_{42}, d_{52}, d_{f2}, r_{p2}, r_{12}, r_{52}, r_{f2}\} \quad (8a)$$

$$\mathscr{D}_{C_2} = \theta_{r12} + \theta_{r22} + \theta_{r32} = \frac{\pi}{2}, \theta_{r42} + \theta_{r52} = \frac{\pi}{2}, \quad d_{12} < 50, r_{f2} \geq -120 \text{ mm} \quad (8b)$$

For avoidance of the parallel singularity condition (6), the following design constraint need to be satisfied where r_{13} for leg 3 is the corresponding parameter to r_{12} of leg 2:

$$r_{12} \neq r_{13} \quad (9)$$

It should be kept in mind that out of the design parameters in $\mathscr{D}_{P_1}$ and $\mathscr{D}_{P_2}$, all the parameters are not independent. The assembly in the reference configuration, as shown in Fig. 1, imposes six independent constraints for each leg. But at the start, it is not possible to identify which parameters should be assumed independent. Hence, the entire set of design parameters is considered at the beginning of the algorithm.

4.2 Parameterization of the End-Effector of the 2T2R PM

The homogeneous matrix representing the end-effector reference frame is :

$${}^0T_f = \begin{bmatrix} m_{11} & 0 & m_{13} & p_x \\ m_{21} & m_{22} & m_{23} & p_y \\ m_{31} & m_{32} & m_{33} & 0 \\ 0 & 0 & 0 & 1 \end{bmatrix} \quad (10)$$

where the terms m_{12} and p_z are zero. The former represents the constraint 1-$\hat{\$}^{\infty}$ provided by the legs 2 and 3, which restrict one DOF of rotation and the latter represents the constraint 1-$\hat{\$}^{0}$ provided by the leg 1, which restricts the translation of the entry point E along the z-axis. Overall there are four independent parameters in the homogeneous matrix corresponding to the four DOFs of the 2T2R manipulator. The column vector $\begin{bmatrix} m_{13} & m_{23} & m_{33} \end{bmatrix}^T$ represents the components of the vector $\mathbf{z_f}$ attached to the end-effector and coincident with the needle axis. The origin O_f is chosen at the entry point $E = (p_x, p_y)$ on the needle axis. The operational coordinates m_{13}, m_{23}, p_x, p_y are chosen as the four independent parameters which describe the configuration of the end-effector. These four operational parameters would be utilized to plot and discuss the workspace boundaries of the 2T2R PM and its legs.

5 APPLICATION

A typical orientation range for percutaneous procedures lies within a cone of axis $\mathbf{z_b}$ with a 30 deg half-angle, whereas a typical translational range is within a circular area of diameter 40 mm centered at O_b. Let us denote these desired orientation and translation workspaces by W_O and W_t for further referencing. The structural parameters of the 2T2R PM are sought, which would lead to at least same size of workspace. For percutaneous procedures, the size of the orientation workspace is more important than the size of the translational workspace. Hence, for each leg, the orientation workspace is discussed first and then the resulting constraints are applied to obtain the translational workspace.

5.1 Workspace Analysis of Leg 1

In this and the next subsection, the expressions for the singularities Eqn. (2) to Eqn. (5) are reformulated to allow for the representation in terms of the DH parameterization. The developed expressions will be utilized to discuss the workspace boundaries and the formation of voids. Reformulating the Singularity-11 described by Eqn. (2) and considering the intermediate reference frames of leg 1 leads to:

$$\mathbf{x_{41}} \cdot \mathbf{z_{31}} = 0 \quad (11)$$

Copyright © 2014 by ASME

Downloaded From: http://proceedings.asmedigitalcollection.asme.org/ on 06/15/2018 Terms of Use: http://www.asme.org/about-asme/terms-of-use

However the angle between $\mathbf{x_{41}}$ and $\mathbf{z_{31}}$ does not represent directly any angle from the DH parameters of the leg 1. The following equality for the intermediate reference frames of DH parameterization holds and can easily be proved :

$$\mathbf{x_{31}} \times \mathbf{x_{41}} = (\mathbf{x_{41}} \cdot \mathbf{z_{31}})\mathbf{z_{41}}. \tag{12}$$

Now substituting Eqn. (11) into Eqn. (12), Eqn. (13a) is obtained.

$$\mathbf{x_{31}} \times \mathbf{x_{41}} = 0 \equiv \sin\theta_{41} = 0 \tag{13a}$$
$$-1 \leq \cos\theta_{41} \leq +1 \tag{13b}$$

Using Eqn. (13b) rather than Eqn. (13a) has two advantages. First, it allows to break the singularity locus into two separate curves at the equality. Second, it gives the inequality for avoiding the singularity. Also, a closed-form solution for θ_{41} is known from the solution of the inverse kinematics. Assuming that $\cos\alpha_{51} \neq 0$ the developed expressions for Eqn. (13b), resulting from the solution of inverse kinematics for this leg, are presented below :

$$S_{11a}: \quad -m_{31}\sin\alpha_{f1} - m_{33}\cos\alpha_{f1} + \cos(\alpha_{41} - \alpha_{51}) \geq 0 \tag{14a}$$

$$S_{11b}: \quad -m_{31}\sin\alpha_{f1} - m_{33}\cos\alpha_{f1} + \cos(\alpha_{41} + \alpha_{51}) \leq 0 \tag{14b}$$

Equation (14) clearly identify the parameters affecting the orientation workspace of the leg 1 and is independent of the position of the end-effector. It is difficult to predict which expression represents the outer boundary and which expression represents the void. Plotting with the inverse kinematics model (IKM) is done to clarify that, with the following arbitrary chosen values of the parameters :

$$\alpha_{41} = \frac{\pi}{6} \quad \alpha_{51} = \frac{\pi}{4} \quad \alpha_{f1} = \frac{\pi}{3} \tag{15}$$

Fig. 4(a) shows the inverse kinematics plot where reachable and unreachable points are presented in blue and red colors respectively. In this figure, the formation of void can be clearly seen. Fig. 4(b) shows the plot of Eqn. (14a) and Eqn. (14b) at equality, where the void and the external workspace boundary are presented in black and green colors respectively. Same color convention will be applied through rest of the paper for describing external boundaries, voids and IKM plots. Thus, two separate

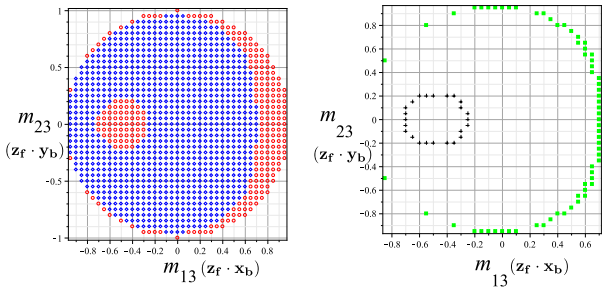

(a) IKM Plot (b) Boundary Plot

FIGURE 4: TYPICAL ORIENTATION WORKSPACE OF THE LEG 1.

equations are obtained for the leg 1, which control the behavior of the outer workspace boundary and the void. Hence from Eqn. (14a), the condition $\alpha_{41} = \alpha_{51}$ can be obtained for the void-avoidance. From Eqn. (7b) and Eqn. (14b), the condition $\alpha_{41} + \alpha_{51} = \frac{\pi}{2}$ can be obtained for the optimization of the external boundary. Thus it solves for two structural parameters of leg 1, which gives $\alpha_{41} = \alpha_{51} = \frac{\pi}{4}$.

After substituting the values of the α_{41} and α_{51} in equations Eqn. (14a) and Eqn. (14b), a point $[m_{13} = \sin\alpha_{f1}, m_{23} = 0]$ and a line $m_{13} = \cos\alpha_{f1}$ are obtained, respectively for the internal and the external singularities, as shown in Fig. 5. The inverse kinematics plots and the plots obtained from the analytical expressions are superimposed. The important thing to notice here is that, though the area of the void has been eliminated, there is still a singular point inside the workspace. The desired orientation workspace W_O is obtained as the brown circular area which keeps a distance of 15 deg from either singularity.

Upon reformulating Singularity-21 described by Eqn. (3),

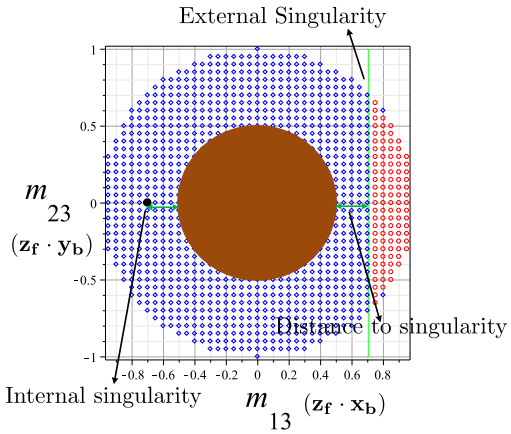

FIGURE 5: DESIRED ORIENTATION WORKSPACE OF THE LEG 1, $\alpha_{f1} = \frac{\pi}{4}$.

Copyright © 2014 by ASME

Downloaded From: http://proceedings.asmedigitalcollection.asme.org/ on 06/15/2018 Terms of Use: http://www.asme.org/about-asme/terms-of-use

the condition Eqn. (16a) is obtained.

$$\mathbf{x_{11}} \times \mathbf{x_{21}} = 0 \equiv \sin\theta_{21} = 0 \quad (16a)$$
$$-1 \leq \cos\theta_{21} \leq +1 \quad (16b)$$

The inequalities in the Eqn. (16b) are presented below for the 2T2R PM in a constant orientation chosen from the reference configuration :

$$S_{21a}: \quad (p_x - p_{xc})^2 + (p_y - p_{yc})^2 \geq (d_{31} - d_{21})^2 \quad (17a)$$
$$S_{21b}: \quad (p_x - p_{xc})^2 + (p_y - p_{yc})^2 \leq (d_{31} + d_{21})^2 \quad (17b)$$

This is the trivial case of an elbow singularity. From Eqn. (17a), it is evident that the void is canceled for $d_{31} = d_{21}$. Equation (17) taken at equality is plotted for the following values of the parameters, in the Fig. 6, which include the constraints derived from the optimization of the orientation workspace :

$$\alpha_{41} = \alpha_{51} = \alpha_{f1} = \frac{\pi}{4} \quad d_{21} = d_{31} = 50 \text{ mm} \quad (18)$$

With above values of the parameters, $p_{xc} = -50$ mm and $p_{yc} = 50$ mm is obtained. The achieved translational workspace is the brown circular area of diameter 40 mm as shown in Fig. 6 and keeps a minimum distance of approximately 10 mm from either singularity.

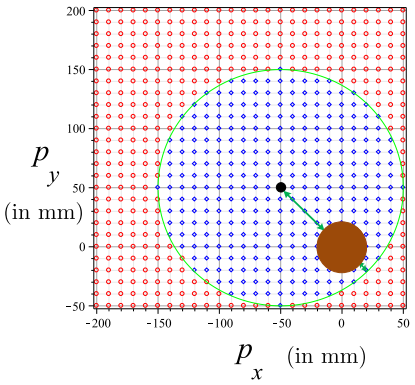

FIGURE 6: DESIRED TRANSLATIONAL WORKSPACE OF THE LEG 1.

The dependent structural parameters obtained after solving the system of equations , arising from assembling the leg 1 in the reference configuration as shown in Fig. 1, are :

$$\theta_{31} = \theta_{41} = \theta_{51} = 1.99 \text{ rad} \quad (19a)$$
$$d_{41} = -24.80 \quad r_{31} = 66.22 \quad r_{41} = -93.65 \text{ mm} \quad (19b)$$

5.2 Workspace Analysis of Legs 2 and 3

The analysis of leg 2 would be carried out in a different manner than the leg 1, as some of the obtained analytical expressions have a more complex form and the two singularities of leg 2 are coupled to each other. The Fig. 7 shows the IKM plot of leg 2 for the orientation workspace with the following arbitrary chosen values of parameters :

$$r_{p2} = 0, r_{12} = -43.30, r_{52} = 1.05, r_{f2} = -120 \text{ mm}$$
$$d_{12} = 25, d_{22} = 35, d_{32} = 35, d_{42} = 10, d_{52} = 77.13 \text{ mm}$$
$$d_{f2} = 56.52 \text{ mm} \quad (20)$$

Reformulating the Singularity-12, as described by Eqn. (4) and considering the intermediate reference frames of leg 2, provides the condition Eqn. (21a):

$$\mathbf{x_{42}} \cdot (\mathbf{z_{42}} \times \mathbf{z_{32}}) = 0 \equiv \cos\theta_{42} = 0 \quad (21a)$$
$$-1 \leq \sin\theta_{42} \leq +1 \quad (21b)$$

The developed expressions for Eqn. (21b) can be written as:

$$S_{12a}: \; d_{52} + r_{12} + d_{f2}\sqrt{1 - m_{13}^2} + m_{13} r_{f2} \geq p_x \quad (22a)$$
$$S_{12b}: \; -d_{52} + r_{12} + d_{f2}\sqrt{1 - m_{13}^2} + m_{13} r_{f2} \leq p_x \quad (22b)$$

To ensure Eqn. (22) produces real values at equality for every point in the desired translational workspace W_t, following condition Eqn. (23) must be fulfilled :

$$Discr = -p_x + r_{12} - d_{52} + \sqrt{d_{f2}^2 + r_{f2}^2} \geq 0 \quad (23)$$

where $Discr$ is the discriminant of the quadratic equation in m_{13} obtained from Eqn. (22b) at equality. To ensure that condition Eqn. (23) is satisfied for the range, -20 mm $\leq p_x \leq 20$ mm, it is assumed that Eqn. (23) is at equality for $p_x = 22$ mm. Hence, the following condition is obtained.

$$Discr = -22 + r_{12} - d_{52} + \sqrt{d_{f2}^2 + r_{f2}^2} = 0 \quad (24)$$

Reformulating Singularity-22, which is described by Eqn. (5), leads to equation Eqn. (25a).

$$\mathbf{x_{12}} \times \mathbf{x_{22}} = 0 \equiv \sin\theta_{22} = 0 \quad (25a)$$
$$S_{22a}: \; \cos\theta_{22} \geq -1 \quad S_{22b}: \; \cos\theta_{22} \leq +1 \quad (25b)$$

Copyright © 2014 by ASME

Downloaded From: http://proceedings.asmedigitalcollection.asme.org/ on 06/15/2018 Terms of Use: http://www.asme.org/about-asme/terms-of-use

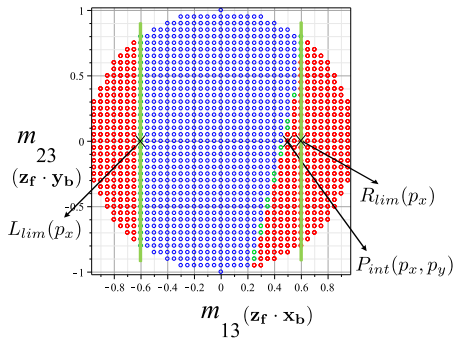

FIGURE 7: TYPICAL ORIENTATION WORKSPACE OF THE LEG 2.

The full expression for S_{22b} is too complex to be detailed here and it is a function of all four operational parameters.

In Fig. 7, three separate singularity curves can be clearly seen, which in fact are plots of Eqn. (22a), Eqn. (22b) and Eqn. (25b) at the equality. S_{22a}, which represents the collapsed position of the elbow singularity, is not present as the typical condition ($d_{22} = d_{32}$) in Eqn. (20) removes any voids within the workspace. The boundary values (L_{lim}, R_{lim}, P_{int}) indicated in the Fig. 7 are the values of m_{13}, which is the limiting factor for obtaining the W_O.

L_{lim} and R_{lim} are obtained from the term S_{12a} and S_{12b} at the equality, respectively and they are function of p_x only. P_{int} is obtained from the intersection of the term S_{22b} at equality with the line $m_{23} = 0$. It is function of both p_x and p_y. To solve for the desired orientation and translational workspaces W_O and W_t, algebraic equations are formed based on these boundary values and then solved for the DH parameters of leg 2, as discussed further in this subsection. Variation of the above boundary values with respect to p_x and p_y is :

$$\frac{\partial L_{lim}}{\partial p_x} < 0, \frac{\partial R_{lim}}{\partial p_x} < 0, \frac{\partial P_{int}}{\partial p_x} < 0, \frac{\partial P_{int}}{\partial p_y} > 0 \qquad (26)$$

Hence, the worst case scenarios are given below at the boundary of the desired translational workspace W_t, where $m_{13lim} = 0.5$ corresponds to size of the desired orientation workspace W_O :

$$L_{lim}(-20 \text{ mm}) = -m_{13lim} \quad R_{lim}(+20 \text{ mm}) = m_{13lim},$$
$$P_{int}(+20 \text{ mm}, -20 \text{ mm}) = m_{13lim} \qquad (27)$$

The following independent parameters were chosen before solving the system of equations for legs 2 and 3:

$$(d_{12} = 50, d_{13} = -50), d_{42} = d_{43} = 5, r_{p2} = r_{p3} = 20$$
$$(r_{12} = -20, r_{13} = -10), r_{f2} = r_{f3} = -120 \text{ mm} \qquad (28)$$

Solving for the rest of the dependent parameters with Eqn. (7b), Eqn. (24), Eqn. (27), Eqn. (28) and the equations derived from the assembly of the legs 2 and 3 in reference configuration as shown in Fig. 1, the unknown parameters in Eqn. (8a) are obtained:

$$\theta_{r_{12}} = 1.44, \theta_{r_{13}} = 1.70, \theta_{r_{22}} = 2.44, \theta_{r_{23}} = -2.54$$
$$\theta_{r_{32}} = -2.32, \theta_{r_{33}} = 2.41, \theta_{r_{42}} = -.04, \theta_{r_{43}} = -.15,$$
$$\theta_{r_{53}} = 1.61, \theta_{r_{52}} = 1.72 \; rad \qquad (29a)$$

$$r_{52} = -21.36, r_{53} = 37.51, d_{32} = 47.47, d_{33} = 23.27,$$
$$d_{52} = 80.26, d_{53} = 90.26, d_{f2} = d_{f3} = 23.39 \text{ mm} \qquad (29b)$$

The desired common W_O obtained for the legs 2 and 3 is shown in Fig. 8 and 9 for different values of p_x and p_y, as the brown circular area. As it can be seen that even in worst scenarios depicted in Fig. 9(a) and 9(b), the desired orientation workspace W_O is obtained for every point in the translational workspace W_t.

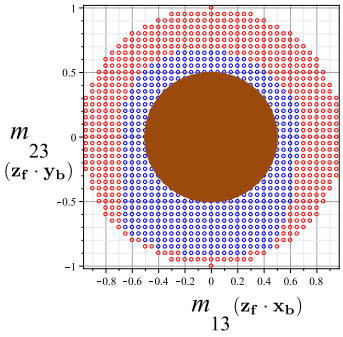

FIGURE 8: COMMON ORIENTATION WORKSPACE W_O OF THE LEGS 2 and 3 at $(p_x, p_y) = (0, 0)$.

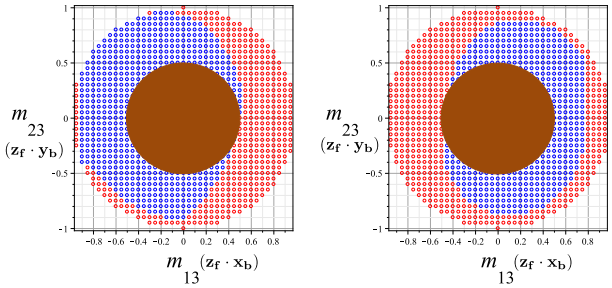

(a) $p_x = 20, p_y = -20$ mm (b) $p_x = -20, p_y = -20$ mm

FIGURE 9: COMMON ORIENTATION WORKSPACE W_O OF THE LEGS 2 and 3.

Copyright © 2014 by ASME

Downloaded From: http://proceedings.asmedigitalcollection.asme.org/ on 06/15/2018 Terms of Use: http://www.asme.org/about-asme/terms-of-use

6 RESULTS

The important structural parameters which determine the size of the base and height of the 2T2R PM in its reference configuration are:

$$d_{12} = d_{21} = 50, d_{13} = -50 \text{ mm}, \tag{30a}$$

$$r_{12} = -20, r_{13} = -10, r_{f2} = r_{f3} = -120 \text{ mm} \tag{30b}$$

Here d_{12}, $|d_{13}|$ and $|r_{f2}|$ represent the size of the base and height of the mechanism, respectively. Hence, the height and base size of the mechanism are limited to a characteristic dimension of 120 mm which were put as the design constraints at start of the dimensional synthesis.

The 2T2R PM was designed for singularity free W_O and W_t workspace. The independent structural parameters were identified for the voids. The conditions for avoiding them are : $\alpha_{41} = \alpha_{51} \quad d_{21} = d_{31} \quad d_{22} = d_{32} \quad d_{23} = d_{33}$.

The Fig. 10(a) and 10(b) show a preliminary prototype without actuators set in the reference and in an arbitrary configuration, respectively. The fabricated prototype of the 2T2R PM holds a 16 G (approx. 1.7 mm diameter) 200 mm long biopsy needle.

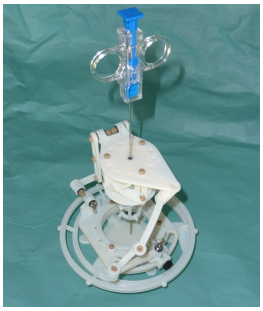

(a) Reference Configuration

(b) In arbitrary configuration

FIGURE 10: PRELIMINARY PROTOTYPE.

7 CONCLUSION AND FUTURE WORK

A novel 2T2R PM was presented for the targeted application of needle manipulation in percutaneous procedures with its advantages over the current designed robotic systems for the same task. An integrated dimensional synthesis algorithm which includes i) the generation of the workspace ii) the identification and the localization of the sensitive structural parameters to each singularity iii) the identification and the elimination of the voids was used for determining the structural parameters of this 2T2R PM. Hence, the study of the effect of each structural parameter individually over the workspace size was not necessary. Furthermore, it would not be computationally viable given the large number of structural parameters for this 2T2R PM. The algorithm for the dimensional synthesis focused more on the screw theory based inspection than the computation of Jacobian matrices for deriving the serial and parallel singularity conditions. The systematic division of singularities into voids and external boundaries as well as the derivation of the inequality expressions for avoiding singularities is presented in this paper for the first time. As a result of this dimensional synthesis, a very compact 2T2R PM was obtained with the required workspace size for the application.

However, this analysis is limited to mechanisms with revolute joints only but can be extended to prismatic joints by considering the joint limits. As illustrated in this paper, this method can be specially effective for the dimensional synthesis of lower mobility mechanisms, where the operational parameters are fewer in number. Also, the algorithm presented will be simpler to implement for special type of workspaces like constant orientation workspace or constant translational workspace, where it is possible to reduce the coupling between structural parameters of different legs. The next steps in the design of this 2T2R PM will be the integration of actuators and the refinement of the mechanical design to obtain the desired stiffness.

ACKNOWLEDGMENT

The authors acknowledge the support of the Image-guided Hybrid Surgery Institute (IHU Strasbourg) and the Foundation ARC. This work has been sponsored by the French government research program Investissements d'Avenir through the Robotex Equipment of Excellence and Labex CAMI (ANR-10-EQPX-44 and ANR-11-LABX-0004).

REFERENCES

[1] Piccin, O., Barbé, L., Bayle, B., Mathelin, M. d., and Gangi, A., 2009. "A force feedback teleoperated needle insertion device for percutaneous procedures". *The International Journal of Robotics Research,* ***28***(9), Sept., pp. 1154–1168.

[2] Walsh, C. J., Hanumara, N. C., Slocum, A. H., Shepard, J.-A., and Gupta, R., 2008. "A patient-mounted, telerobotic tool for CT-Guided percutaneous interventions". *Journal of Medical Devices,* ***2***(1), p. 011007.

[3] Hungr, N., Fouard, C., Robert, A., Bricault, I., and Cinquin, P., 2011. "Interventional radiology robot for CT and MRI guided percutaneous interventions.". In MICCAI (1), G. Fichtinger, A. L. Martel, and T. M. Peters, eds., Vol. 6891 of *Lecture Notes in Computer Science*, Springer, pp. 137–144.

Copyright © 2014 by ASME

Downloaded From: http://proceedings.asmedigitalcollection.asme.org/ on 06/15/2018 Terms of Use: http://www.asme.org/about-asme/terms-of-use

[4] San Martin, J., Trivino, G., and Bayona, S., 2007. "Mechanical design of a minimally invasive surgery trainer using the manipulability as measure of optimization". In ICM2007 4th IEEE International Conference on Mechatronics, pp. 1–5.

[5] Li, J., Liu, Y., Wang, C., and Sun, L., 2006. "Optimal kinematic design of a planar parallel manipulator with high speed and high precision". In Proceedings of the 2006 IEEE International Conference on Mechatronics and Automation, pp. 1888–1892.

[6] Ravani, B., and Roth, B., 1983. "Motion synthesis using kinematic mappings". *Journal of Mechanical Design,* ***105***(3), Sept., pp. 460–467.

[7] Hayes, M. J. D., and Husty, M. L., 2003. "On the kinematic constraint surfaces of general three-legged planar robot platforms". *Mechanism and Machine Theory,* ***38***(5), May, pp. 379–394.

[8] Purwar, A., and Gupta, A., 2011. "Visual synthesis of rrr- and rpr-legged planar parallel manipulators using constraint manifold geometry". In ASME 2011 International Design Engineering Technical Conferences and Computers and Information in Engineering Conference, American Society of Mechanical Engineers, pp. 1081–1092.

[9] Wu, J., Ge, Q. J., Su, H.-J., and Gao, F., 2012. "Kinematic acquisition of geometric constraints for task-oriented design of planar mechanisms". *Journal of Mechanisms and Robotics,* ***5***(1), Oct., pp. 011003–011003.

[10] Kumar, N., Piccin, O., and Bayle, B., 2014. "A task-based type synthesis of novel 2T2R parallel mechanisms". *Mechanism and Machine Theory,* ***77***, July, pp. 59–72.

[11] Maurin, B., Bayle, B., Piccin, O., Gangloff, J., de Mathelin, M., Doignon, C., Zanne, P., and Gangi, A., 2008. "A patient-mounted robotic platform for CT-scan guided procedures". *IEEE transactions on bio-medical engineering,* ***55***(10), Oct., pp. 2417–2425. PMID: 18838367.

[12] Zhang, Y., and Ting, K., 2012. "Type synthesis of uncoupled 2T2R parallel manipulators". In Proceedings of the ASME 2012 International Design Engineering Technical Conferences & Computers and Information in Engineering Conference IDETC/CIE, pp. 505–511.

[13] Li, Q., and Huang, Z., 2003. "Type synthesis of 4-DOF parallel manipulators". In IEEE International Conference on Robotics and Automation, 2003. Proceedings. ICRA '03, Vol. 1, pp. 755–760 vol.1.

[14] Dai, J. S., Huang, Z., and Lipkin, H., 2006. "Mobility of overconstrained parallel mechanisms". *Journal of Mechanical Design,* ***128***(1), p. 220.

[15] Merlet, J. P., 2006. *Parallel Robots*. Springer.

[16] Agrawal, S., 1991. "Workspace boundaries of in-parallel manipulator systems". In , Fifth International Conference on Advanced Robotics, 1991. 'Robots in Unstructured Environments', 91 ICAR, pp. 1147–1152 vol.2.

[17] Khalil, W., and Kleinfinger, J., 1986. "A new geometric notation for open and closed-loop robots". In 1986 IEEE International Conference on Robotics and Automation. Proceedings, Vol. 3, pp. 1174–1179.

Copyright © 2014 by ASME

Downloaded From: http://proceedings.asmedigitalcollection.asme.org/ on 06/15/2018 Terms of Use: http://www.asme.org/about-asme/terms-of-use